Available online at www.sciencedirect.com
ScienceDirect
Journal of Luminescence 128 (2008) 1205–1210
JOURNAL OF LUMINESCENCE
www.elsevier.com/locate/jlumin

The luminescence properties of the ZnO@$ZnWO_4$:Eu^{3+} core–shell composites

Qilin Dai[a,b], Hongwei Song[a,b,*], Guohui Pan[a,b], Xue Bai[a,b], Hui Zhang[a,b], Ruifei Qin[a,b], Lanying Hu[a,b], Haifeng Zhao[a,b], Shaozhe Lu[a,b], Xinguang Ren[a,b]

[a]*Key Laboratory of Excited State Physics, Changchun Institute of Optics, Fine Mechanics and Physics, Chinese Academy of Sciences, 16 Eastern Nan-Hu Road, Changchun 130033, PR China*
[b]*Graduate School of Chinese Academy of Sciences, 16 Eastern Nan-Hu Road, Changchun 130033, PR China*

Received 20 March 2007; received in revised form 29 October 2007; accepted 29 November 2007
Available online 5 December 2007

Abstract

The ZnO@$ZnWO_4$:Eu^{3+} core–shell composites were prepared by a two-step hydrothermal method and the photoluminescence properties of the composites were studied in contrast to the corresponding hexagonal ZnO and monoclinic $ZnWO_4$: Eu^{3+} nanocrystals prepared by the one-step hydrothermal method. The results demonstrate that in the nanocomposites the Eu^{3+} ions in the $ZnWO_4$ phase occupy two symmetry sites, one a well-crystalline inner site and one a disordered surface site; while in the $ZnWO_4$: Eu^{3+} nanocrystals, the local environments surrounding Eu^{3+} ions are relatively disordered for both the inner and the surface sites. This indicates that in the composites, the crystallinity of the $ZnWO_4$ becomes better, which have positive influence on the improvement of photoluminescence. The temperature stabilities for both the emissions of ZnO and Eu^{3+} ions are improved in contrast to the pure ZnO or $ZnWO_4$:Eu^{3+} nanocrystals.

Keywords: Core–shell nanocomposite; Luminescence; Energy transfer

1. Introduction

As a wide direct band gap (~3.3 eV) semiconductor, ZnO has been attracting much attention due to its potential applications in short-wavelength ultraviolet (UV) laser and blue-green optoelectronic devices [1–3]. The large exciton binding energy (~60 meV) permits exciton recombination well above room temperature. Laser under optical excitation has been experimentally demonstrated at room temperature [1–3]. As an important photoelectronic material, one-dimensional (1-D) ZnO nanomaterials also attracted extensive interests in the past decade. Especially, ZnO UV-nanowire laser under optical pumping was realized at room temperature by Huang et al. [2]. To date, different techniques have been used to prepare nanocrystalline ZnO, such as the electrodeposition method, the vapor transport method, the vapor deposition method, the vapor–liquid–solid process, the wet chemical method and so on. The photoluminescence properties of semiconductors, such as the luminescence of excitons or deep levels (DLs) of defects depend on the preparation techniques strongly [3].

Rare earths doped in the ZnO host may realize novel functions in some electro-optical devices and thus have attracted considerable attention; however, it is difficult to dope rare earths into the ZnO lattices. Recently, composite materials attracted much attention, especially the core–shell structure, which not only can improve the primary properties but also can create some novel functions [4–6]. It is known that tungstate is a very important family of inorganic material that has a high potential application in various fields [7], such as photoluminescence [8], microwave

*Corresponding author at: Key Laboratory of Excited State Physics, Changchun Institute of Optics, Fine Mechanics and Physics, Chinese Academy of Sciences, 16 Eastern Nan-Hu Road, Changchun 130033, PR China. Tel.: +86 431 6176 320; fax: +86 431 8617 6320.
E-mail address: hwsong2005@yahoo.com.cn (H. Song).

0022-2313/$ - see front matter © 2007 Elsevier B.V. All rights reserved.
doi:10.1016/j.jlumin.2007.11.093

applications [9], optical fibers [10], scintillator materials [11] and so on. As a self-activating phosphor, tungstate has some advantages, e.g. high chemical stability, high average refractive index, high X-ray absorption coefficient, high efficiency output, short decay time and low afterglow to luminescence [12]. There are two types of structures in tungstates: wolframite and scheelite. Zinc tungstate has the wolframite structure, which is monoclinic with space group P2/c. The luminescence properties of zinc tungstate have been extensively investigated because it is a widely used scintillation crystal [8,13–15]. In rare earth-doped tungstates, excited tungstate groups emit blue-green lights themselves under ultraviolet excitation. At the same time, the excited tungstate group may also effectively transfer energy to rare earths such as trivalent europium and samarium, generating red emissions [16,17]. Therefore, some rare earth-doped tungstates become potential white-light phosphors. In the past few years, there appeared many literatures corresponding to the preparation and photoluminescence properties of rare earth-doped tungstates nanocrystals. It is expected that in the ZnO@$ZnWO_4$:Eu^{3+} core–shell composites, some novel energy transfer processes such as the energy transfer from tungstates to ZnO or from ZnO to europium could be realized and the photoluminescence properties of ZnO or $ZnWO_4$:Eu^{3+} could be improved. In addition, Eu^{3+} ion owns super-sensitive *f–f* transitions, which is an ideal luminescence probe to study the local environments, giving the detail of the core–shell structure. Here we report the preparation, characterization and photoluminescence properties of the ZnO@$ZnWO_4$:Eu^{3+} core–shell composites.

2. Experiments

2.1. Sample preparation

All chemicals were analytic-grade reagents without further purification. In a typical synthesis, 2 mmol NaOH aqueous solution was added into 1 mmol $Zn(CH_3COO)_2 \cdot 2H_2O$ aqueous solution under magnetic stir to obtain the corresponding suspension, and then the resultant suspension was transferred into 12 Teflon-lined stainless-steel autoclaves (50 ml) averagely and maintained at 150 °C for 12 h. After the reaction, the Teflon-lined autoclaves were cooled naturally to room temperature. Then the white precipitate was collected and washed with deionized water. Finally, the white product (ZnO rods) was obtained by centrifugation and dried at 80 °C in a vacuum condition for 2 h.

In the preparation of the ZnO@$ZnWO_4$:Eu^{3+} composites, firstly, 0.5 mmol ZnO nanorods prepared by the hydrothermal method were redispersed into deionized water and kept with vigorous stirring for 2 h. Then, 0.25 mmol Na_2WO_4 and $Eu(CH_3COO)_3$ solutions (0.005 mmol) were added into the above solution. The pH value of the mixture was adjusted with addition of HNO_3 or NaOH solution in a dropwise manner, followed by further stirring for 2 h. Resultant milky suspensions with a pH value of about 8 were finally given another hydrothermal treatment at 150 °C for 12 h in one autoclave. Powders were finally obtained (the doping concentration was 2 mol%) after washing with deionized water and drying at 80 °C for 2 h in a vacuum oven.

$ZnWO_4$:Eu^{3+} nanocrystals were prepared by the reaction of $Zn(CH_3COO)_2$ and $Eu(CH_3COO)_3$ as well as by Na_2WO_4 for 12 h at a certain temperature (150 °C) with pH = 8. In a typical procedure, $Eu(CH_3COO)_3 \cdot 4H_2O$, $Zn(CH_3COO)_2 \cdot 2H_2O$ and $Na_2WO_4 \cdot 2H_2O$ were dissolved in deionzed water, respectively. Then the former two solutions were mixed together (1 mmol $Zn(CH_3COO)_2$ and 0.02 mmol $Eu(CH_3COO)_3$), and then appropriate Na_2WO_4 (1 mmol) was added with vigorous stirring. The pH value of the mixed solution was adjusted with addition of CH_3COOH or NaOH solution in a dropwise manner. After that, the solution was added into a Teflon-lined stainless-steel autoclave of 50.0 ml capacity. The autoclave was kept at 150 °C for 12 h. Afterwards, the autoclave was cooled to room temperature gradually. Then the white precipitate was collected and washed with deionized water several times. The solid was heated at 80 °C and dried under vacuum for 2 h, finally the white powders of $ZnWO_4$:Eu^{3+} (the doping concentration was 2 mol%) were obtained.

2.2. Measurements

Field emission scanning electron microscopy (FE-SEM) was taken on a HITACHI S-4800 electron microscope. The electron diffraction pattern was obtained with a JEM-2010 transmission electron microscope (TEM) made by Japanese JEOL Company. X-ray diffraction (XRD) data were collected on a Rigaku D/max-rA X-ray diffractometer using a Cu target radiation source. Emission and excitation spectra were recorded at room temperature using a Hitachi F-4500 spectrophotometer equipped with a continuous 150 W Xe-arc lamp. For comparison of different samples, the emission spectra were measured at a fixed bandpass of 0.2 nm with the same instrument parameters (2.5 nm for the excitation slit, 2.5 nm for the emission slit and 700 V for the PMT voltage). In the measurements of the temperature-dependence of emission intensity, the samples were placed into a liquid nitrogen cycling system, in which the temperature varied from 77 to 300 K. The 325 nm light that came from a He–Cd laser was used for excitation. The spectra were recorded by UV-Lab Raman infinity with a resolution of 2 cm^{-1}. The experiments of frequency-selective excitation were performed at 77 K, in which the samples were placed into a liquid-nitrogen system. A Rhodamine 6G dye pumped by the Nd:YAG laser was used as the frequency-selective excitation source. It is with a line width of 0.2 cm^{-1}, pulse duration of 10 ns and a repetition frequency of 10 Hz. A Spex 1403 spectrometer and a Boxcar integrator were used to record the emission spectra.

3. Results and discussion

3.1. Characterization

Fig. 1(a)–(c) shows the FE-SEM images of ZnO, $ZnWO_4$:Eu^{3+} and ZnO@$ZnWO_4$:Eu^{3+} samples, respectively, and (d) shows the energy dispersive X-ray detector (EDX) of the ZnO@$ZnWO_4$:Eu^{3+} composite. From the SEM images ZnO powders yield nanorods, having an average diameter of ~100 nm and length of ~500 nm. The $ZnWO_4$:Eu^{3+} powders yield nanoparticles of 10–20 nm in diameter. The size and shape of the ZnO@$ZnWO_4$:Eu^{3+} composite have no obvious change in comparison with the ZnO nanorods, except that the surface of the composite becomes rough. The enlarged image in inset of Fig. 1(c) demonstrates that there exist some nanoparticles on the surface of the ZnO nanorods. The electron diffraction pattern from one nanoparticle on the surface of the composite indicates that the nanoparticles are monoclinic in phase, clearly implying that the $ZnWO_4$ nanoparticles are formed on the surface of the ZnO nanorods. The shape and the size of the nanoparticles on the surface of the composite are nearly identical with those shown in Fig. 1(b). From the EDX of the composite, it can be seen that the composite contains W and Eu elements besides Zn and O, which further indicates the forming of ZnO@$ZnWO_4$:Eu^{3+} composites. Fig. 2 shows the XRD patterns of the ZnO nanorods, $ZnWO_4$:Eu^{3+} nanoparticles and ZnO@$ZnWO_4$:Eu^{3+} composites. It can be seen that $ZnWO_4$:Eu^{3+} nanocrystals are monoclinic in phase (JCPDS No. 73-0554) and the ZnO nanorods are hexagonal in phase (JCPDS No. 80-0074) and the phase of the composites is the same with that of ZnO nanorods. This indicates that in the composites the amount of $ZnWO_4$:Eu^{3+} is relatively less.

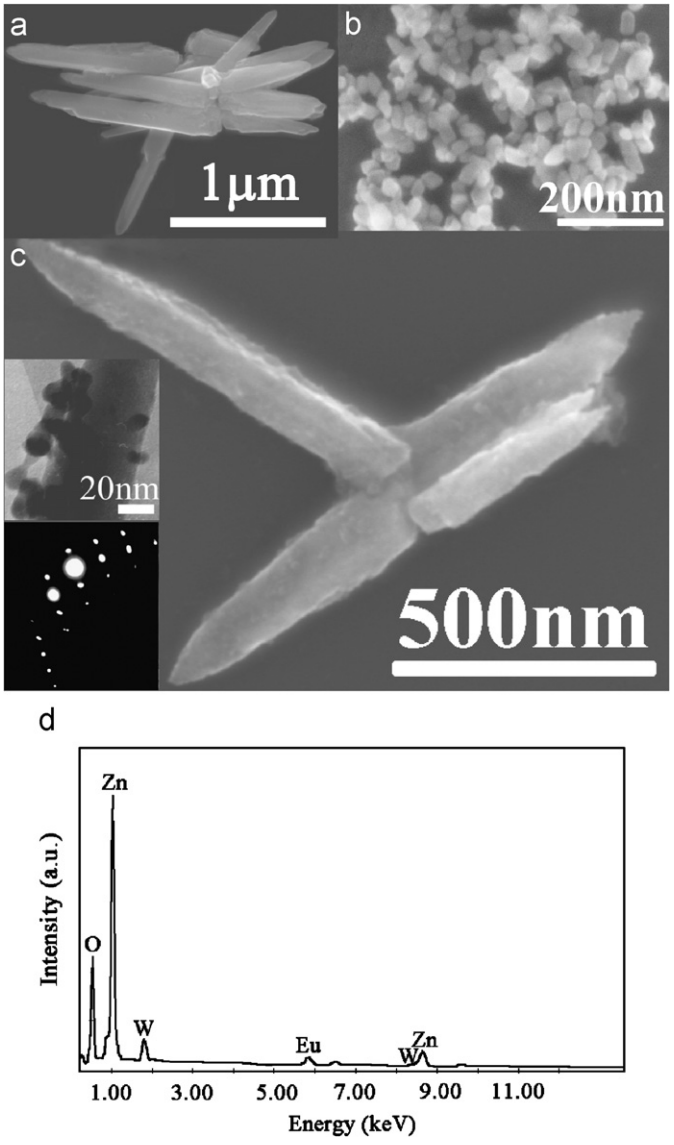

Fig. 1. FE-SEM images of the samples: (a) the ZnO nanorods; (b) $ZnWO_4$:Eu^{3+} nanoparticles; (c) the ZnO@$ZnWO_4$:Eu^{3+} composites; and (d) the EDX of the composites; the inset, the TEM of a single nanorod of the composite and the SAED of a nanoparticle on the surface.

3.2. Photoluminescence properties

Fig. 3a shows the emission and excitation spectra of the $ZnWO_4$:Eu^{3+} nanoparticles and ZnO@$ZnWO_4$:Eu^{3+} composites. From the spectra of the $ZnWO_4$:Eu^{3+} nanocrystals, the absorption of the tungstate group can be decomposed into two Gaussian components: one located at ~260 nm (peak A) and the other at ~325 nm (peak B). Peak A is assigned to the transitions of tungstate at normal lattice sites, while peak B to the transitions at perturbed phases [18]. These perturb sites may be tungstate ions next to either chemical or structural defects and thus have a different symmetry and crystal-field strength than tungstate ions in normal lattice site. Some authors ascribed it to the transitions in a tungstate group, which lacked one oxygen ion [18]. In the composites, only the peak at ~260 nm appears, while the peak at ~325 nm disappears. It is suggested that in the composites the energy transfer from the disturbed tungstate to ZnO occurred. In other words, the absorption energy by the disturbed tungstate group was not transferred to Eu^{3+} but transferred to ZnO. Fig. 3b

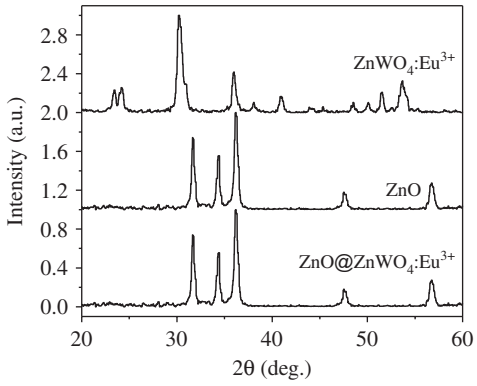

Fig. 2. XRD pattern of the $ZnWO_4$:Eu^{3+} particles, ZnO nanorods and the ZnO@$ZnWO_4$:Eu^{3+} composites.

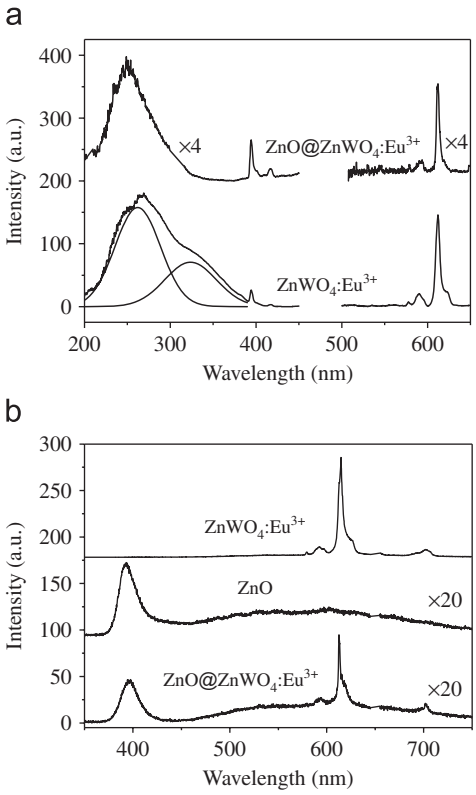

Fig. 3. (a) Room-temperature excitation spectra (left part) ($\lambda_{em} = 612$ nm) and emission spectra (right part) ($\lambda_{ex} = 260$ nm) of Eu^{3+} in the composite and the $ZnWO_4$:Eu^{3+} nanocrystals. (b) The emission spectra for the composite under the excitation of the 325 nm He–Cd laser.

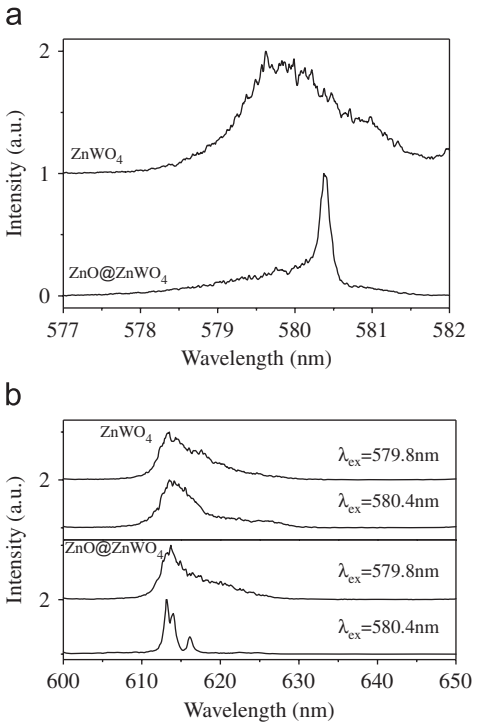

Fig. 4. (a) $^7F_0$–$^5D_0$ excitation spectra ($\lambda_{em} = 613$ nm) and (b) $^5D_0$–$^7F_2$ emission spectra by selectively exciting $^7F_0$–$^5D_0$ transitions (at 77 K) in $ZnWO_4$:Eu^{3+} nanocrystals and the ZnO@$ZnWO_4$:Eu^{3+} composites.

shows the emission spectra of the composites in contrast to the ZnO and $ZnWO_4$:Eu^{3+} nanocrystals under the excitation of the 325 nm laser at room temperature. It can be seen that ZnO nanocrystals have two emission peaks, a narrower peak at ~394 nm and a broader peak at ~591 nm. The 394-nm peak originates from the recombination of excitons, while the 591-nm peak from the recombination emission between the conduction band or shallow donors and interstitial oxygen (O_i), which acts as a deep-level (DL) O_i center [19,20]. In the composites, beside the emission bands originated from ZnO, the $^5D_0$–^7F_J, sharp lines for the Eu^{3+} ions also appear, having a main peak at 610 nm.

Generally, the $^5D_0$–$^7F_0$ transition of Eu^{3+} is parity-forbidden, but when Eu^{3+} ions occupy one of Cs, Cn, Cnv; the transition will be partially allowed and can be detected. Because the $^5D_0$–$^7F_0$ line has no splitting at any crystal field, it is suitable to study the site symmetry surrounding Eu^{3+} ions. Fig. 4(a) and (b) shows, respectively, $^7F_0$–$^5D_0$ excitation spectra ($\lambda_{em} = 613$ nm) and the $^5D_0$–$^7F_2$ emission spectra by selectively exciting $^7F_0$–$^5D_0$ transitions of the ZnO@$ZnWO_4$:Eu^{3+} composites and the $ZnWO_4$:Eu^{3+} nanocrystals. A broader excitation line at 579.8 nm was observed in $ZnWO_4$:Eu^{3+} nanocrystals, while a sharper line at 580.4 nm accompanied with a broader tail at 579.8 nm was observed in the composites. This indicates that the local environments surrounding the Eu^{3+} ions in the composites are neater in contrast to the $ZnWO_4$ nanocrystals, which is ascribed to the better crystallinity of $ZnWO_4$ synthesized by chemical corrosion [21]. The Eu^{3+} should locate in the $ZnWO_4$ lattices instead of the ZnO ones. In fact, we used the same method to prepare ZnO:Eu^{3+} crystals, but no photoluminescence of Eu^{3+} was observed, suggesting that Eu^{3+} was not doped into the ZnO lattices. The excitation lines at 580.4 and 579.8 nm in the composites are attributed to the photoluminescence of Eu^{3+} located at two different sites, the inner and the surface sites, respectively [22]. In many nanocrystalline systems, the nanoparticles comprise of a well-crystalline core and a relatively disordered surface [23]. In the present $ZnWO_4$:Eu^{3+} nanocrystals, no matter the inner and the surface Eu^{3+} ions locate at relatively disordered environments, which cannot be distinguished in the excitation spectra. The emission spectra in Fig. 4(b) demonstrate the same facts. In fact, the better crytsallinity of the $ZnWO_4$ lattices in the ZnO@$ZnWO_4$:Eu^{3+} composites will lead to the improvement of luminescence quantum yield. However, because the content of $ZnWO_4$:Eu^{3+} in the composites is quite low, the intensity of Eu^{3+} in the composites decreases in comparison to $ZnWO_4$:Eu^{3+}.

It is interesting to observe that in the ZnO@$ZnWO_4$:Eu^{3+} composites the thermal stability of the photoluminescence becomes better compared to that in the $ZnWO_4$:Eu^{3+} nanocrystals, for the emissions of both ZnO and Eu^{3+}. The temperature–dependence of photoluminescence under 325 nm excitation in the ZnO@$ZnWO_4$:Eu^{3+} composites, $ZnWO_4$:Eu^{3+} nanoparticles and ZnO nanorods

is drawn in Fig. 5. From Fig. 5(a) and (b) it can be seen that the exciton emission of ZnO nanoparticles tends to decrease with the elevated temperature, while in the composites it tends to increase. This further suggests that in the composites the energy transfer from $ZnWO_4$ to ZnO probably occurs. Generally, the increased temperature leads the energy transfer processes to be more effective. From Fig. 5(c) and (d) it can be seen that the defect emission of ZnO decreases with elevated temperature, for both ZnO nanocrystals and the ZnO@$ZnWO_4$:Eu^{3+} composites; however, in the composites the emission drops more slowly. For the red emission caused by ZnO deep defect levels, the intensity as a function of temperature is well fitted by the well-known thermal activation function [24],

$$I(T) = \frac{I_0}{1 + \alpha e^{E_A/k_B T}}, \quad (1)$$

where I_0 is the emission intensity at 0 K, α is the proportional coefficient, E_A is the thermal activation energy, k_B is Boltzmann's constant and T is the absolute temperature. The values of α obtained by fitting for the ZnO@$ZnWO_4$:Eu^{3+} composites and ZnO nanocrystals are 15.89 and 3.03, respectively, and the values of E_A are 57.6 and 18.4 meV. It is obvious that the thermal stability of the ZnO defect emissions in the composites is much better than that in the ZnO nanoparticles. In Fig. 5(e) and (f) it is seen that the emission of Eu^{3+} in the $ZnWO_4$:Eu^{3+} nanocrystals decreases with the increase of temperature, while that in the composites has only a little variation, which indicates that in the composites the thermal stability for the emission of Eu^{3+} is better than that in the $ZnWO_4$:Eu^{3+} nanocrystals.

The increase of thermal stability for the emission of ZnO in the composites could be attributed to the following two points: the possible energy transfer from $ZnWO_4$ to ZnO and the modified surface of ZnO nanorods by $ZnWO_4$. In the nanocrystals, a number of surface adsorptions such as OH^- and CO_3^{2-} bonds were involved, which acted as luminescence-quenching centers. As the temperature increases, the nonradiative energy transfer from ZnO to them increases, leading to the temperature quenching. In the composites, the surface modification with tungstate blocks the surface nonradiative channels. Moreover, the tungstate has strong adsorption at 325 nm, which could transfer energy to the ZnO host.

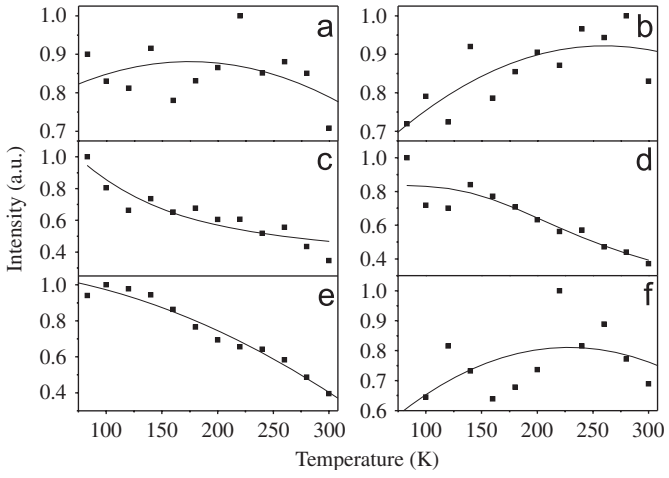

Fig. 5. Dependence of emission intensity on temperature in different samples: (a) the exciton emission in the ZnO nanorods ($\lambda_{em} = 394$ nm); (b) the exciton emission in the ZnO@$ZnWO_4$:Eu^{3+} composites ($\lambda_{em} = 394$ nm); (c) the defect emission in the ZnO nanorods ($\lambda_{em} = 591$ nm); (d) the defect emission in the composites ($\lambda_{em} = 591$ nm); (e) the emission of Eu^{3+} in $ZnWO_4$:Eu^{3+} nanocrystals and ($\lambda_{em} = 610$ nm) (f) the emission of Eu^{3+} in the composites ($\lambda_{em} = 610$ nm).

The increase of thermal stability for the emission of Eu^{3+} in the composites can be mainly attributed to neater local environments surrounding Eu^{3+}; in other words, this means a better crystallinity of $ZnWO_4$ lattices, which has been identified by the site-selective excitation spectra. The neater local environments could avoid unexpected energy transfer processes from tungstate or Eu^{3+} to some defect levels. The improved crystallinity of $ZnWO_4$ lattices in the composites is related to the preparation processes. On the one hand, in the composites the $ZnWO_4$ lattices were formed through chemical corrosion, in which the tungstate groups combined with Zn^{2+} ions belonging to the ZnO lattices. In the process, the $ZnWO_4$ lattices were formed gradually, so the growing of $ZnWO_4$ was rather slow compared to the direct synthesis of $ZnWO_4$. On the other hand, the existence of crystal seed (ZnO) ensure that sufficient Zn^{2+} source existed in the growing process, which would decrease the inner and the surface dangling bonds.

4. Conclusions

ZnO@$ZnWO_4$:Eu^{3+} core–shell composites were prepared by chemical corrosion via a two-step hydrothermal method and characterized by TEM images, electron diffractions and XRD patterns. The photoluminescence properties of the composites were studied in contrast to ZnO and $ZnWO_4$:Eu^{3+} nanocrystals prepared by the one-step hydrothermal method. The results demonstrate that the energy transfer from the $ZnWO_4$ to ZnO probably happens in the core–shell composites. In the nanocomposites, Eu^{3+} occupies two symmetry sites, the well-crystalline inner site and the more disordered surface site; while in the $ZnWO_4$:Eu^{3+} nanocrystals, the local environments surrounding Eu^{3+} ions are relatively disordered for both the inner and the surface sites. This implies better crystallinity of the $ZnWO_4$ synthesized by chemical corrosion. The temperature–dependence of photoluminescence suggests that the thermal stability for both the emissions of ZnO and Eu^{3+} ions is improved in contrast to the pure ZnO or $ZnWO_4$:Eu^{3+} nanocrystals.

Acknowledgments

The corresponding author thanks the financial support by National Natural Science Foundation of China (Grants

55772042, 10704073 and 10504030) and National Key Project of China (863).

References

[1] Z.K. Tang, G.K.L. Wang, P. Yu, M. Kawasaki, A. Ohtomo, H. Koinuma, Y. Segawa, Appl. Phys. Lett. 72 (1998) 3270.
[2] M. Huang, S. Mao, H. Feick, H. Yan, Y. Wu, H. Kind, E. Weber, R. Russo, P. Yang, Science 292 (2001) 1897.
[3] Z. Qiu, K.S. Wong, Appl. Phys. Lett. 84 (2004) 2739.
[4] R.A. Caruso, M. Antonietti, Chem. Mater. 13 (2001) 3272.
[5] M. Yu, J. Lin, J. Fang, Chem. Mater. 17 (2005) 1783.
[6] Z. Jiang, C.J. Liu, Phys. Chem. B 107 (2003) 1241.
[7] B. Chamberland, J. Kafalas, J. Goodenough, Inorg. Chem. 16 (1977) 44.
[8] T. Takagi, J. Fukazawa, Appl. Phys. Lett. 36 (1980) 278.
[9] L. Uitert, S. Preziosi, J. Appl. Phys. 33 (1962) 2908.
[10] H. Wang, F. Medina, Y. Zhou, Q. Zhang, Phys. Rev. B 45 (1992) 10356.
[11] K. Tanaka, T. Miyajima, N. Shirai, Q. Zhang, R. Nakata, J. Appl. Phys. 77 (1995) 6581.
[12] Z. Lou, J. Hao, M. Cocivera, J. Lumin 99 (2002) 349.
[13] Y. Pisarevskii, L. Silvestrova, R. Voszka, A. Peter, Phys. Rev. B 43 (1990) 10356.
[14] P. Born, D. Robertson, P. Smith, G. Hames, J. Reed, J. Telfor, J. Lumin 24/25 (1981) 131.
[15] H. Grassmann, H. Moser, J. Lumin 33 (1985) 109.
[16] M. Treadaway, R. Powell, Phys. Rev. B 15 (1975) 862.
[17] F. Wen, X. Zhao, H. Huo, J. Chen, E. Lin, J. Zhang, Mater. Lett. 55 (2002) 152.
[18] M.J.J. Lammers, G. Blasse, D.S. Robertson, Phys. Stat. Sol. A 63 (1985) 59.
[19] A.B. Djurisic, Y.H. Leung, W.C.H. Choy, K.W. Cheah, W.K. Chah, Appl. Phys. Lett. 84 (2004) 2635.
[20] X.L. Wu, G.G. Siu, C.L. Fu, H.C. Ong, Appl. Phys. Lett. 78 (2001) 2285.
[21] G. Pan, H. Song, X. Bai, L. Fan, H. Yu, Q. Dai, B. Dong, R. Qin, S. Li, S. Lu, X. Ren, H. Zhao, J. Phys. Chem. C III (2007) 12472.
[22] H. Peng, H. Song, B. Chen, S. Lu, S. Huang, Chem. Phys. Lett. 370 (2003) 485.
[23] S. Mintova, N.H. Olson, V. Valtchev, T. Bein, Science 283 (1999) 958.
[24] B. Li, Y. Liu, Z. Zhi, D. Shen, Y. Lu, J. Zhang, X. Fan, J. Cryst. Growth. 240 (2002) 479.